J Appl Electrochem (2009) 39:1643–1649
DOI 10.1007/s10800-009-9854-x

ORIGINAL PAPER

Nano-porous SiO/carbon composite anode for lithium-ion batteries

Wei-Ren Liu · Yu-Chan Yen · Hung-Chun Wu · Martin Winter · Nae-Lih Wu

Received: 1 May 2008 / Accepted: 25 February 2009 / Published online: 12 March 2009

Abstract Carbon-coating of sub-μm SiO particles ($d_{max} = 0.36$ μm, $d_{50} = 0.69$ μm) by a fluidized-bed chemical-vapor-deposition process has produced unique nano-porous SiO/C secondary particles within which the SiO primary particles are "glued" together by carbon to form a network that possesses randomly distributed pores with sizes in the nano-meter range and a bulk porosity of >30%. Upon lithiation/delithiation cycling in an organic Li-ion electrolyte, the electrode made of the SiO/C particles exhibited reduced polarization, smaller irreversible electrode expansion, and remarkably enhanced cycling performance, as compared with that of pristine SiO particles. The reduced electrode expansion exhibited by the SiO/C electrode can be attributed to the combination of diluted SiO content and presence of pre-set voids, which could partially accommodate volume expansion arising from lithiation of the SiO primary particles. These effects render the SiO/C electrode structurally more robust than the SiO electrode against volumetric variations upon cycling.

Keywords Lithium ion battery · Anode · SiO · Chemical vapor deposition · Carbon coating · Nano-porosity

W.-R. Liu · Y.-C. Yen · N.-L. Wu (✉)
Department of Chemical Engineering, National Taiwan University, Taipei 106, Taiwan, ROC
e-mail: nlw001@ntu.edu.tw

H.-C. Wu
Material and Chemical Research Laboratories, ITRI, Chutung, Hsin-Chu 310, Taiwan, ROC

M. Winter
Institute of Physical Chemistry, University Muenster, 48149 Muenster, Germany

1 Introduction

In order to increase the electrical storage capacity for the Li-ion secondary batteries, a vast amount of research has been devoted to replacing the graphite anode with new materials that form alloys with Li. Among them, Si and Si-containing compounds are of great interest [1–9], owing to their large potential specific capacities, low cost and environment-benign nature. In spite of these advantages, all these anode materials suffer from serious volumetric expansion and contraction during charge/discharge (C/D) cycling. The cyclic variations in dimension tend to cause rapid capacity fading due to deterioration in electrical contacts either between electrode constituent particles or with current collector. For SiO, the performance additionally suffers from poor electronic conductivity, which not only limits rate-capability but also causes energy loss upon cycling.

Miyachi et al. [10] have demonstrated a Li-uptake capacity greater than 2,000 mAh g^{-1} SiO for an amorphous SiO thin-film electrode prepared by vacuum deposition under a C/D current rate of C/40. It was also asserted, based on their X-ray photoelectron spectroscopy analysis, that some (~60%) of Si remains in the oxidized form as lithium silicate phase even in the fully lithiated state. The rate capability and cycle stability of SiO thin-film electrode have recently been markedly improved by incorporating up to 25 wt.% of metals to form a composite structure [11].

For the SiO thick-film electrodes prepared with SiO particles by the conventional slurry-coating technique, Yang et al. [12] once showed initial capacities of ~800 mAh g^{-1} for nano-sized (30–50 nm) SiO particles at a fairly low current density (0.2 mA cm^{-2}) with a cycle life up to 30 cycles. The capacity of the electrode made of

μm-sized SiO particles dropped to less than 600 mAh g^{-1} within 20 cycles. Improved cycle life was reported by adopting mechano-chemical reduction of SiO to form composites with rather complex compositions [13, 14]. Cycle-life enhancement has also been reported for SiO/C composite prepared by ball-milling and high-temperature pyrolysis that leads to extensive disproportionation of SiO into Si and SiO_2 [15]. New design of material structure and composition may pave the way to further enhancement in cycling performance [8, 16].

In this work, SiO was coated with carbon (C) layer for modifying its C/D cycling behaviors. C-coating on Si anode was pioneered by Yoshio et al. [17, 18]. It is demonstrated here that, when sub-μm SiO particles are subjected to C coating in a fluidized-bed chemical-vapor-deposition (CVD) process, the particles tend to be "glued" together by carbon to form a network that possesses randomly distributed pores with sizes in the nano-meter range and a high bulk porosity (>30%). When subjected to charge/discharge cycling against a Li electrode, the electrode made of the porous SiO/C composite particles exhibits remarkably improved cycle life as compared with the electrode of the un-coated SiO particles. The improvement may in part be attributed to the presence of the pre-set voids, which help to accommodate the cyclic volumetric variations arising from lithiation/delithiation of the SiO primary particles.

2 Experimental

SiO (99.9%, Aldrich) particles were wet-ground for size reduction with a planetary mill (Fritsch Pulverisette P7) using zirconia vials and balls. Alcohol was used as the lubricant. After milling at 600 rpm for 5 h, sub-μm SiO powders were obtained. The resulting powders were then coated with C in a fluidized-bed CVD reactor, which was operated at 950 °C with benzene vapor as the carbon source. In a typical run, carrier gas, N_2, was bubbled through a benzene reservoir and then directed to a vertical reactor, where the SiO powder sit. The powder was periodically agitated and tossed with a pulsed flow. During the CVD process, the sub-μm SiO particles tended to form larger secondary particles, which were then gently ground and sieved (−325 mesh) for electrode preparation.

The morphologies of the synthesized SiO/C composite and pure SiO were examined by scanning electron microscopy (SEM; LEO1530), equipped with energy dispersive X-ray (EDX) analysis. To prepare the electrode samples for SEM cross-section examination, cycled cells were carefully opened, and the SiO-containing electrodes were thoroughly rinsed with dimethyl carbonate (DMC) in a glove box. The rinsed electrodes were first placed in the glove box for initial drying and then in a vacuum desiccator for further drying and storage before analyses. The electrodes were transferred into the SEM chamber without vacuum protection, although the exposure time to air has been reduced as possible. Particle size distribution was determined by light scattering analysis (LS-230; Coulter). The measurements of porosity and pore size distribution were carried out by Mercury porosimetry (AutoPore 9500 IV). The carbon content of the coated SiO particles was determined by elemental analysis (Heraeus varioIII-NCSH). Transmission electron microscopy (TEM) analysis was conducted with a field-emission transmission electron microscope (FE-TEM, JEOL JEM-2100F). To prepare the TEM specimen, the secondary particles were mounted within an epoxy matrix, and cross-section slices were prepared by microtomy.

The tested electrodes consisted of (on a dry basis) 62 wt.% of either SiO/C composite or SiO, 30 wt.% of conductive additives and 8 wt.% of binder. The binder was a mixture of styrene–butadiene–rubber (SBR; L1571, Asahi Chemicals) and sodium-carboxyl-methyl-cellulose (SCMC; WS-C, Cellogen, DKS International, Inc.) with 1:1 weight ratio. The conductive additives included graphitic flakes (KS-6, 3 μm, TIMCAL) and nano-sized carbon black (Super P, 40 nm, TIMCAL) with a weight ratio of 5:1. The mixed-slurry was coated onto a Cu-foil and dried in a vacuum oven at 150 °C. The SiO and SiO/C electrodes were assembled into CR2032 coin cells for electrochemical characterizations. The counter electrode was lithium foil. All the voltage differences reported herein are referenced to the Li-foil counter electrode. The electrolyte was 1 M $LiPF_6$ in ethylene carbonate (EC): ethyl methyl carbonate (EMC) (1:2 vol.%) from Mitsubishi Chemical Corporation. The C/D tests were carried out with a constant current-constant voltage mode within the voltage range from 10 to 1,200 mV. The constant-current phase employed a current of 0.15 A g^{-1} (the current density is based on the active material only, either SiO/C or SiO), while the constant-voltage phase was fixed at 10 mV with a cut-off current of 0.05 A g^{-1}.

3 Results and discussion

3.1 Microstructural characterization

The as-received SiO powder had a size distribution that peaked at ~30 μm (curve 1, Fig. 1), as determined by light scattering, and contained ~92% of the particles with a size between 10 and 100 μm. The SiO particles after milling show a size distribution peaked at 0.36 μm with d_{50} of 0.69 μm (curve 2, Fig. 1). After the CVD process, the sub-μm particles were found to agglomerate together to form

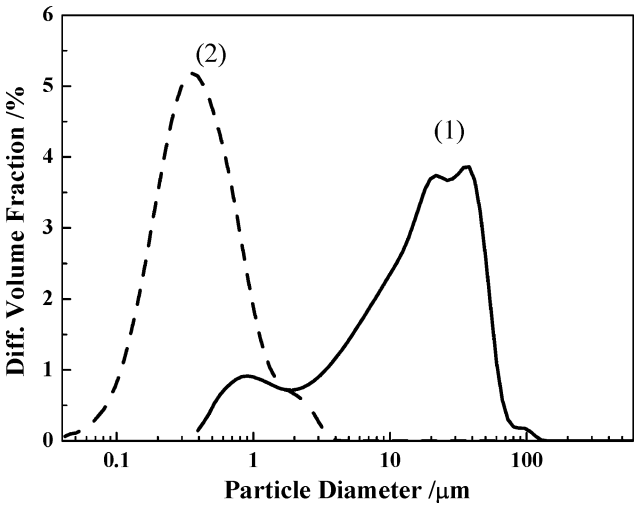

Fig. 1 Particle size distributions of SiO (1) before and (2) after high-energy ball-milling for 5 h

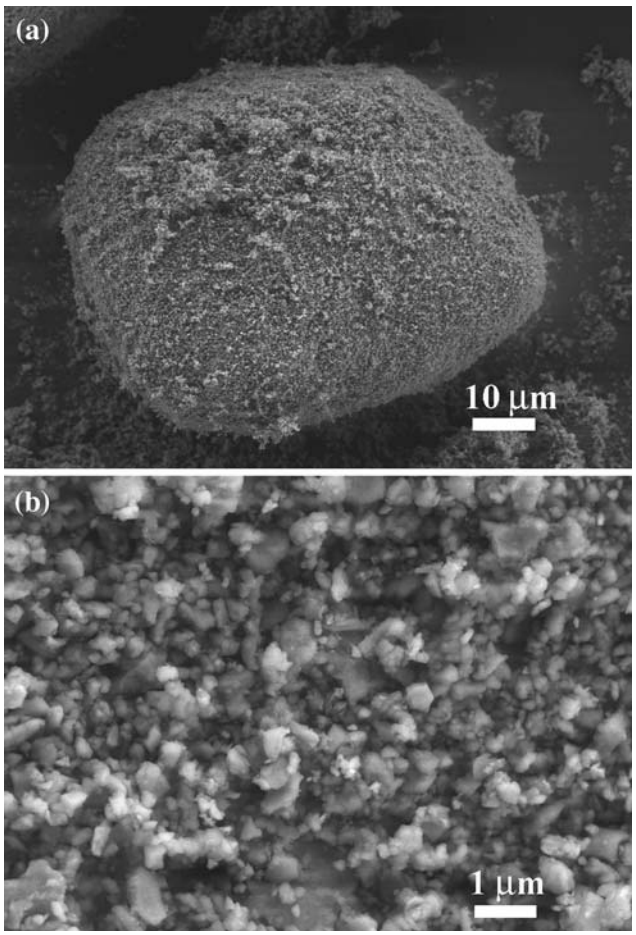

Fig. 2 SEM micrographs of SiO/C composite powder: **a** a SiO/C secondary particle, and **b** the SiO primary particles constituting the secondary particle shown in (**a**)

much larger SiO/C secondary particles (Fig. 2a). SEM analysis shows that the secondary particles are composed of smaller particles with sizes not larger than 0.5 μm (Fig. 2b).The amount of carbon within the composite powder, as determined by the elemental analysis, was 29 wt.%. Previous Raman study has confirmed that the C coating produced under the present condition is partially (~50%) graphitic in nature [7]. Figure 3 compares the XRD patterns of the SiO powder before and after the C-coating process. The SiO powder remains mostly amorphous, as indicated by the strong hump within $2\theta = 20$–$30°$. A set of very weak Si peaks was detected, suggesting very limited (<10% as estimated based on the peak intensity) extent of disproportionation of SiO. There were additionally a set of tetragonal ZrO_2 peaks after the CVD process. The oxide contaminant must has come from the grinding medium (ZrO_2 balls) and sintered to form larger crystallites during the CVD process. EDX analysis indicated a Zr:Si atomic ratio of 2.0 (±0.3) %, which corresponded to 5.6 wt.% ZrO_2 in the ground SiO powder.

TEM examination of the cross-section slices of the secondary SiO/C particles showed that the SiO particles were predominantly in the range 0.1–0.5 μm in size (Fig. 4a, b). Thus, the light scattering data and the SEM and TEM observations are basically consistent with one another concerning the primary SiO particle size. Furthermore, the TEM micrographs (e.g., Fig. 4b), along with EDS analysis, also revealed conformal coverage of the SiO particles with layered, as well as filamentous, C coating, and randomly distributed voids between the particles (the voids are mostly filled with TEM mounting material, epoxy). Some particles showing dark contrast gave a strong Zr signal. They are believed to be the ZrO_2 crystallites as detected by the XRD. As shown, they exist only in small amounts.

The bulk porosity of SiO/C composite powder was determined by mercury intrusion (Fig. 5). The pore

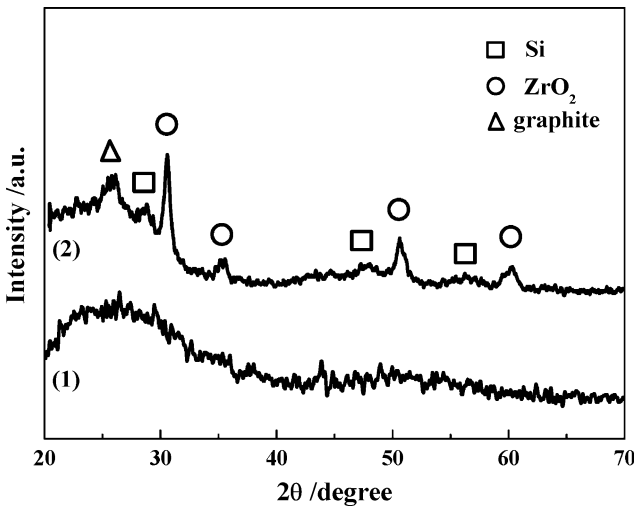

Fig. 3 XRD patterns for SiO powder (curve 1) before and (curve 2) after C-coating at 900 °C

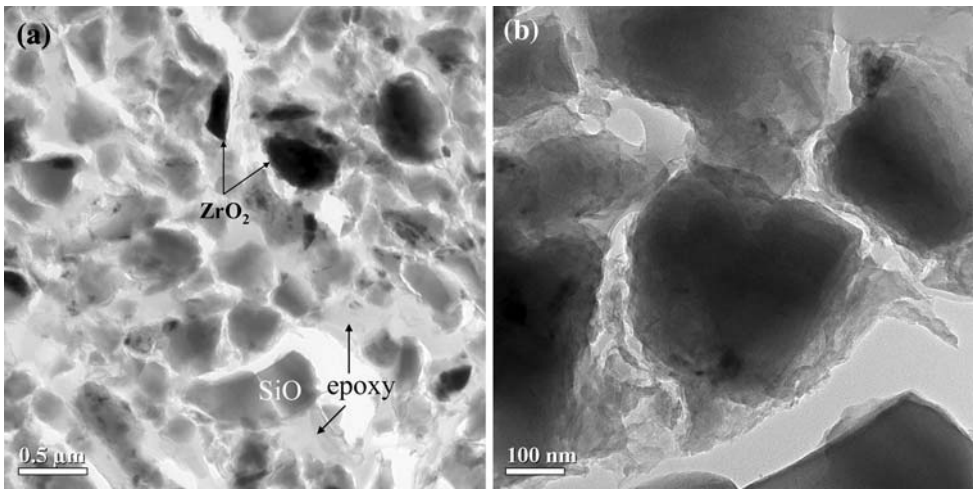

Fig. 4 Cross-section TEM micrographs of the SiO/C composite secondary particles. The semi-transparent film-like material shown in (**a**) and (**b**) is epoxy, the mounting material for preparing the sliced specimen

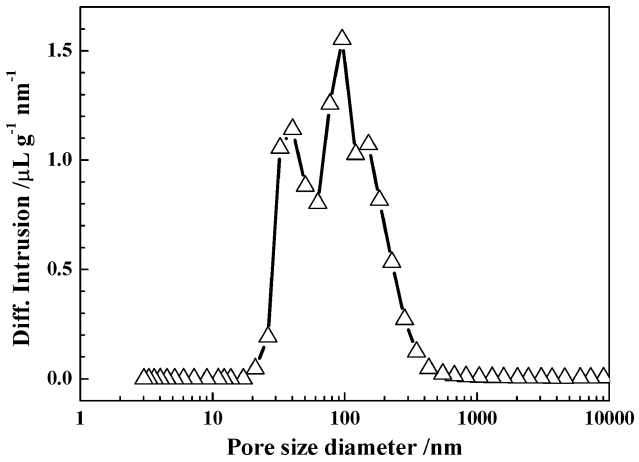

Fig. 5 Pore diameter distribution for SiO/C composite powder as measured by mercury intrusion analysis

diameter distribution peaked at 100 nm with more than 90% pore volume within the range <300 nm. The pore diameters are within the same range as those revealed by TEM (e.g., Fig. 4a). Thus, the measured pore volume is predominantly within the secondary particles (i.e., the intra-particle pores). The total intra-particle pore volume for the composite powder is determined to be 0.223 mL g^{-1}. The density of the pristine SiO particles is 2.13 g mL^{-1} (the manufacturer's value), and the density of the carbon coating may be approximated by the graphite value (2.25 g mL^{-1}). The SiO/C secondary particles are thus estimated to have a bulk porosity of ~32%. It is worthy mentioning that the porous secondary particles described herein could not be obtained when another μm-sized SiO powder (d_{max} = ~3 μm) was employed for the CVD process. That is, the agglomeration process during the CVD process is unique to the sub-μm SiO powder. It is no surprise to find the SiO primary particle size to be a critical factor in the formation of the porous agglomerates, as particle agglomeration is known to be favored by smaller particles.

3.2 Electrochemical characterizations

During the first discharge (the term "discharge" refers to lithiation of SiO, while "charge" delithiation), the SiO electrode showed first a reduction plateau near 200 mV, followed by a sloped curve (curve 1, Fig. 6a). The (dQ/dV) plot (curve 1, Fig. 7), where Q is capacity and V voltage, identified a strong reductive peak at 194 mV and two more weak peaks at 72 and 44 mV, respectively. The 194 mV-peak corresponds to the plateau shown in the voltage curve (Fig. 6a) and is due to the lithiation of SiO [19]. The other two weak peaks are due to lithiation of KS6, as confirmed by a control study using a KS-6 anode. Upon charge, the voltage curve (Fig. 6a) showed an inclined oxidation plateau between 200 and 600 mV. The charge (dQ/dV) plot (curve 2, Fig. 7) shows three oxidation peaks, which have a one-to-one correspondence with the reduction peaks.

During the first discharge of the SiO/C electrode, lithiation commenced above 900 mV (Fig. 6b), in contrast to ~600 mV for the SiO electrode. This additional lithiation has previously also been observed for the C-coated Si electrode, and can be attributed to the lithiation of disordered carbon within the C coating, as revealed by impedance study [7]. A SiO reduction plateau also occured near 200 mV but with a smaller capacity than that shown by the SiO electrode. This is reflected by a significantly weaker SiO reduction peak near 200 mV in the discharge (dQ/dV) plot (curve 3, Fig. 7). In addition, the SiO reduction peak was found to split into two at the tip and occur at a slightly lower voltage, 177 meV, than that of the SiO electrode (194 meV). The peak splitting along with the voltage shift may signal some modification in the internal structural of the SiO particles. The nature of the modification is not clear at this point but might be related to the disproportionation

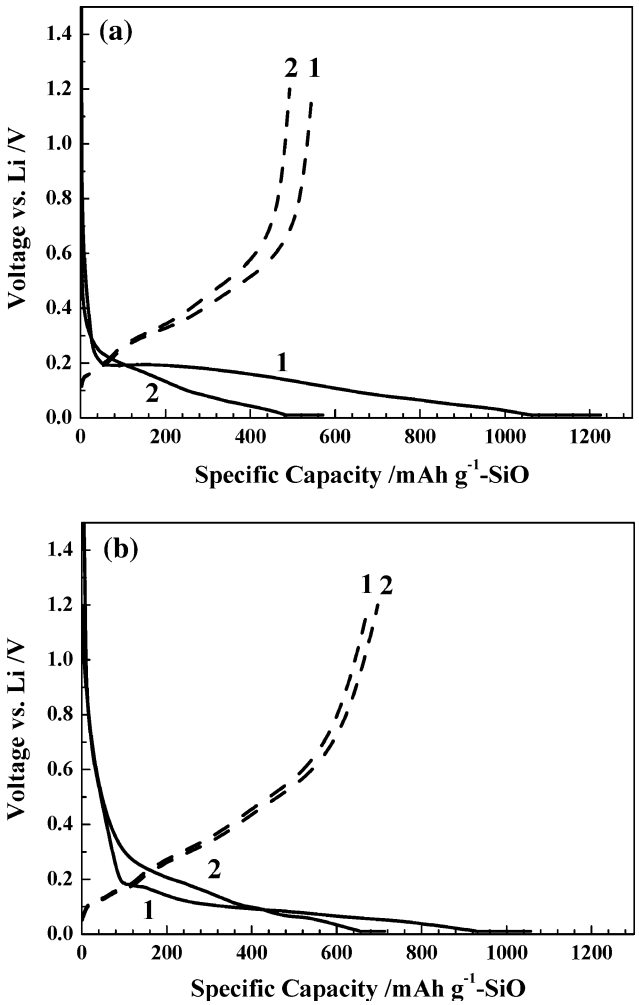

Fig. 6 Voltage curves of the first and second cycles for **a** SiO electrode and **b** SiO/C electrode

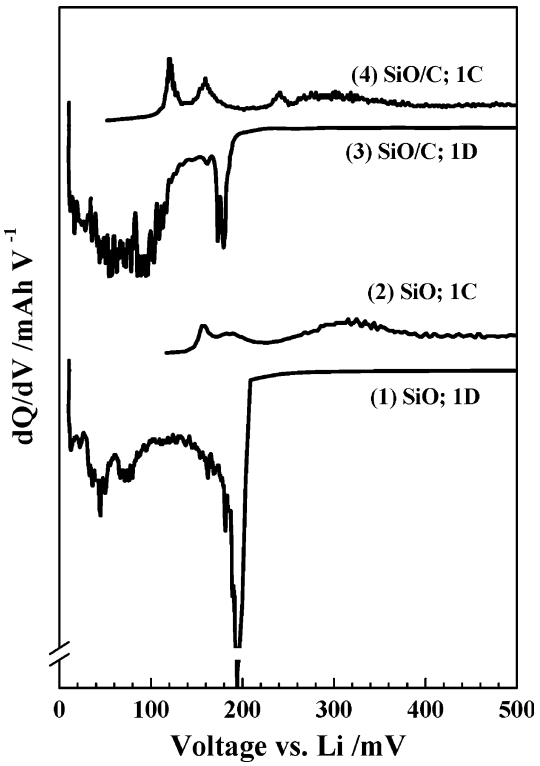

Fig. 7 The (dQ/dV) plots for (1) the first discharge of the SiO electrode; (2) first charge, SiO; (3) first discharge, SiO/C; (4) first charge, SiO/C

reaction of SiO during the CVD process [15]. The two KS-6 reduction peaks were seen at lower potentials. Upon charge (curve 4, Fig. 7), all the oxidation peaks of the SiO/C electrode appeared better resolved than those of the SiO electrode. Two SiO oxidation peaks were in fact observed, echoing with the doublets at the tip of the reduction counterpart. Furthermore, it was noted that the voltage difference between peaks of each redox-pair was significantly smaller for the SiO/C electrode (60–70 mV) than for the SiO one (110–120 mV). This may indicate that the SiO/C electrode exhibits smaller polarization upon C/D, and hence higher electric conductivity within the electrode. This improvement is apparently due to the presence of the conductive C-coating.

Figure 8 shows the specific capacity based on the active material powder (including ZrO_2 contaminant in the case of SiO/C) versus cycle number. The capacity data have been calculated by subtracting the contribution of KS-6 based on a reversible specific capacity of 309 mAh g^{-1} (KS-6), which has been determined experimentally using a KS-6 electrode under the same C/D conditions. The SiO electrode showed first-cycle discharge and charge capacities of 1,225 and 546 mAh g^{-1}, respectively. The first discharge capacity is less than that ($\sim$2,000 mAh g^{-1}) previously reported for SiO thin-film electrodes [10] but comparable with those of thick-film electrodes [13, 15]. The lower initial discharge capacity exhibited by the thick-film type of electrodes can in general be attributed to their relatively larger oxide particle sizes and greater electrode resistances.

The SiO/C electrode exhibited first-cycle discharge and charge capacities of 1,056 and 675 mAh g^{-1}, respectively. Assuming a specific capacity of 309 mAh g^{-1} also for the C layer, then the first discharge and charge capacity of the SiO component is estimated to be 1,352 and 799 mAh g^{-1} SiO, respectively. The reversible efficiency is 59%, which is significantly higher than that ($\sim$44%) of the SiO electrode.

The irreversible capacity of the first cycle may arise mainly from two causes. Firstly, Miyachi et al. [10] revealed that part of the Li ions inserting into SiO during discharge form lithium silicates and oxide (Li_2O), which cannot be delithiated upon charge. Their mechanism based on XPS data suggested a possible reversibility efficiency of

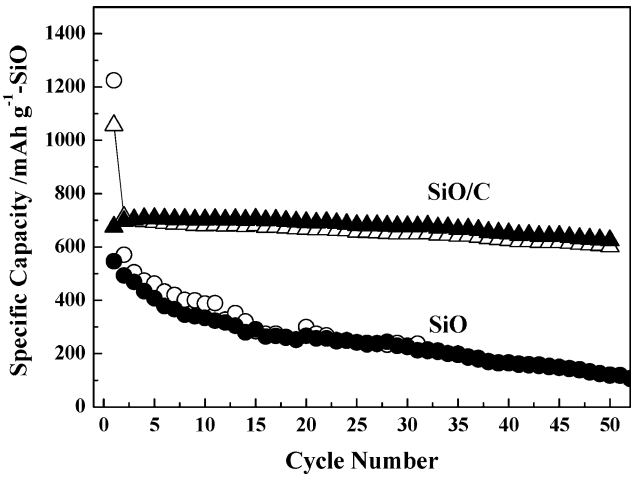

Fig. 8 Capacity versus cycle number. Shown are the discharge capacity (*open symbols*) and charge capacity (*solid symbols*) versus cycle number for SiO/C (Δ, ▲), and SiO (○, ●) electrodes. The specific capacity is based on unit weight of active material, either SiO or SiO/C

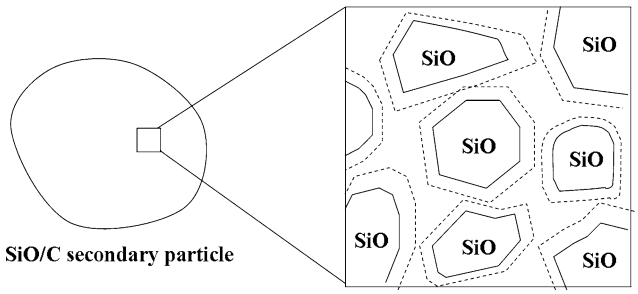

Fig. 9 Schematic drawing to illustrate the ability of intra-particle voids to help to accommodate volumetric expansion of primary SiO particles upon lithiation. The solid and dashed lines delineate the boundaries of the SiO particles before and after lithiation, respectively

∼45% for pure SiO, although a slightly higher reversible efficiency, 50%, was once achieved in a later study [11]. Secondly, the cyclic volumetric expansion and contraction of the SiO particles during the C/D processes may adversely affect electrical connection among the constituent particles within the electrode, causing part of the lithiated SiO particles not to be able to release Li ions upon charging. Based on the values of the reversible efficiencies, it is inferred that, the first-cycle irreversible capacity for the SiO/C, which has an efficiency of 59%, is likely caused predominantly by the silicate-formation effect, while that of the SiO electrode, 44%, may have been affected by both the silicate-formation and volume-expansion effects. The cycling performance data, as described below, have indicated that the SiO/C electrode is indeed more stable against the volume-expansion effect.

Upon cycling, the SiO electrode showed rapid capacity fading, possessing a capacity of merely 120 mAh g^{-1} after 50 cycles. In contrast, the SiO/C electrode exhibited remarkably improved cycle stability (Fig. 8), retaining a capacity of 620 mAh g^{-1}, or 88% of the maximum capacity, after 50 cycles. It is also interesting to note that, for the SiO/C electrode, its charge capacity became slightly higher than the discharge capacity after the second cycle. One possible reason is that some of the Li ions left within the SiO particles upon the completion of the first cycle were gradually released during subsequent cycles, perhaps due to changes either in microstructure or in bulk composition within the particles with cycling. Furthermore, although the SiO/C electrode showed greater discharge capacities and hence greater extents of volume expansion after the second cycle, its capacity faded much slower. The structure of the SiO/C electrode is apparently more robust against the cyclic volumetric variations.

Measurement of the electrode thickness by a micrometer showed that the thickness of the SiO electrode (excluding the thickness of the Cu current collector) increased by an average factor of 3.2, while that of the SiO/C is 1.7. The significantly smaller thickness expansion may explain why the SiO/C electrode is more structurally stable upon cycling. The reduced thickness expansion may result from two main causes. Firstly, there is essentially less SiO content per unit volume in the SiO/C electrode than in the SiO one, i.e., the so-called "dilution" effect. Secondly, as schematically represented in Fig. 9, the pre-set voids existing within the secondary SiO/C particles may be capable of partially accommodating the volume expansion of the primary SiO particles and hence reducing the overall thickness expansion of the electrode. A similar effect has previously been observed in a nano-porous Si/NiSi composite electrode, which was prepared via a completely different synthesis technique [8].

In summary, C-coating of sub-μm SiO particles in a fluidized-bed CVD process was found to produce nano-porous SiO/C composite secondary particles that contain randomly distributed pores in the nano-meter range and a high (>30%) intra-particle porosity. Compared with the SiO particle electrode, the SiO/C particle electrode benefits from reduced polarization and remarkably enhanced cycling performance. The cycle-life improvement is associated with reduced irreversible electrode expansion, and the expansion reduction can in turn be attributed to the combination of diluted SiO content and the presence of pre-set voids. The latter may help to partially accommodate volume expansion arising from lithiation of the SiO primary particles. In spite of the promising improvement in cycle life, the data also suggest that the large irreversible capacity loss arising from the formation lithium silicates and oxide during the first cycle has to be solved by other means before SiO can be a commercially viable anode.

Acknowledgments This work was partially supported by the Industrial Technology Research Institute and by National Taiwan University (contract number 97R0066-09).

References

1. Wen CJ, Huggins RA (1981) J Solid State Chem 37:271
2. Obrovac MN, Christensen L (2004) Electrochem Solid State Lett 7:A93
3. Yagi H, Tarui H (2003) US patent No. 6,649,033 B2
4. Beaulieu LY, Hatchard TD, Bonakdarpour A, Fleischauer MD, Dahn JR (2003) J Electrochem Soc 150:A1457
5. Liu WR, Guo ZZ, Young WS, Shieh DT, Wu HC, Yang MH, Wu NL (2005) J Power Sources 140:139
6. Liu WR, Yang MH, Wu HC, Chiao SM, Wu NL (2005) Electrochem Solid-State Lett 8:A100
7. Liu WR, Wang JH, Wu HC, Shieh DT, Yang MH, Wu NL (2005) J Electrochem Soc 152:1719
8. Liu WR, Wu NL, Shieh DT, Wu HC, Yang MH, Korepp C, Besenhard JO, Winter M (2007) J Electrochem Soc 154:A97
9. Kasavajjula U, Wang C, Appleby AJ (2007) J Power Sources 163:1003
10. Miyachi M, Yamamoto H, Kawai H, Ohta T, Shirakata M (2005) J Electrochem Soc 152:A2089
11. Miyachi M, Yamamoto H, Kawai H (2007) J Electrochem Soc 154:A376
12. Yang J, Takeda Y, Imanishi N, Capiglia C, Xie JY, Yamanoto O (2002) Solid State Ionics 152–153:125
13. Lee HY, Lee SM (2004) Electrochem Commun 6:465
14. Yang X, Wen Z, Xu X, Lin B, Hung S (2007) J Power Sources 164:880
15. Kim JH, Sohn HJ, Kim H, Jeong G, Choi W (2007) J Power Sources 170:456
16. Besenhard JO, Winter M (1997) J Power Sources 68:87
17. Yoshio M, Wang H, Fukuda K, Umeno T, Dimov N, Ogumi Z (2002) J Electrochem Soc 149:A1598
18. Dimov N, Kugino S, Yoshio M (2003) Electrochim Acta 48:1579
19. Tabuchi T, Yasuda H, Yamachi M (2005) J Power Sources 146:507